A magnetically induced self-assembly of Ru@Fe_3O_4/rGO cathode for diclofenac degradation in electro-Fenton process

Bing Qiu, Xiaolan Zhou*, Weimin Li, Houjuan Zhu, Long Yu, Chao Yuan, Rongni Dou, Mingtai Sun, Suhua Wang**

School of Environmental Science and Engineering, Guangdong University of Petrochemical Technology, Maoming 525000, China.

*Corresponding Author's E-mail: zxlzhouxiaolan@163.com; Address: School of Environmental Science and Engineering, Guangdong University of Petrochemical Technology, Maoming 525000, China.

**Corresponding Author's E-mail: wangsh@gdupt.edu.cn; Address: School of Environmental Science and Engineering, Guangdong University of Petrochemical Technology, Maoming 525000, China.

Highlights

- The innovative magnetically assembled electrode (MAE) was used in hetero-EF process.
- Nearly 100% of DCF were degraded by Ru@Fe_3O_4/rGO MAE at current 40 mA within 90 min.
- Ru@Fe_3O_4/rGO MAE showed high activity and stability in hetero-EF process for DCF degradation under pH 2-5.
- $^1O_2$ and •OH were the main ROS participating in DCF degradation in Ru@Fe_3O_4/rGO MAE hetero-EF process.

Abstract

In this study, a novel magnetic nanocomposite of Ru@Fe_3O_4/rGO was successfully synthesized by a simple hydro-thermal method. The Ru@Fe_3O_4/rGO particles were assembled and immobilized for innovative magnetically assembled electrode (MAE) without any binder, and the electrode was further applied in heterogeneous electro-Fenton (hetero-EF) process for the degradation of diclofenac (DCF). The results showed that rGO could remarkably enhance the conductivity and catalyze the two-electron oxygen reduction, which greatly improved the generation of H_2O_2. In addition, the mixture valence of Fe and Ru species might provide rich reaction sites and enhance electron transfer by synergy. Thus, the Ru@Fe_3O_4/rGO MAE exhibited a stable and high electrocatalytic activity in the hetero-EF process for DCF degradation over a wide pH range from 2-9 owing to the higher electroactive surface area (EASA) and lower charge/mass-transfer resistance. The DCF degradation efficiency could reach about 100% within 90 min under pH 5 and current 40 mA, and the Ru@Fe_3O_4/rGO MAE showed high stability and reusability after five cycles. Theoretically, $^1O_2$ and •OH were the main reactive oxygen species (ROS) participating in DCF degradation in the Ru@Fe_3O_4/rGO MAE hetero-EF process. Furthermore, according to the LC-MS/MS intermediates, the possible DCF degradation pathway was deduced including dechlorination, hydroxylation and ring opening attacked by ROS. Eleven intermediates were detected during DCF degradation in the MAE hetero-EF process, and the ecological risk of DCF degradation in Ru@Fe_3O_4/rGO MAE hetero-EF process was significantly reduced. This study provides new insights into the magnetically assembled electrode of Ru@Fe_3O_4/rGO and displays a new practical application prospect of the materials for high-efficient removal and degradation of DCF from wastewater.

Key words: Heterogeneous E-Fenton; Diclofenac; Oxygen reduction reaction; Magnetic assembly; Synergistic activation.

1. Introduction

In recent years, pharmaceutical and personal care products (PPCPs) are produced over 2×10^7 t in the whole world leading to the large quantities discharging into the water. As one of best-known and popular non-steroidal anti-inflammatory drugs (NSAIDs), diclofenac (DCF) can inhibit cyclooxygenase with the properties of antipyretic, analgesic, and anti-inflammatory (Xu et al., 2022; Sharafee Shamsudin et al., 2023). DCF has obvious characteristics of aromatic rings as hydrophobicity and non-biodegradable. The degradation efficiency of DCF in wastewater-treatment plants (WWTPs) is low leading to the accumulation and detection of DCF and its derivatives in surface water, ground water, soil, even in edible fruits and vegetables (Dung Nguyen et al., 2023; Wojcieszyńska et al., 2023). It has been reported that DCF not only has the medication toxicity of chronic and acute, but also pose an adverse ecological risk to non-targeted organisms through biomagnification in the food chain which might increase the ecological risk and directly affect human health (Sathishkumar et al., 2020). Therefore, there is an urgent need to develop effective technology to remove diclofenac in wastewater.

In the past few years, electrochemical advanced oxidation processes (EAOPs) have demonstrated its great ability for the efficiently and thoroughly treatment of refractory wastewater attributing to the high oxidation of reactive oxygen species (ROSs) such as hydroxyl radical (•OH) (Zhou et al, 2020a). Particularly, electro-Fenton (EF) process can in-situ produce hydrogen peroxide (H_2O_2) through two-electron oxygen reduction reaction (ORR) on the cathode, following by the activation by Fe^{2+} to produce •OH (**Eq.** (1-2)). H_2O_2 can be generated continuously avoiding the risk of transport and storage, besides Fe^{2+} could be regenerated which might reduce the production of sludge (**Eq.** (3)) (Li et al., 2023). However, the EF process must operate under acidic conditions with narrow pH range (2.8-3.5) for the activation of H_2O_2 and sluggish of Fe^{2+} recovery limiting its wide application.

$$O_2 + 2e^- + 2H^+ \rightarrow H_2O_2 \quad (1)$$

$$Fe^{2+} + H_2O_2 + H^+ \rightarrow Fe^{3+} + H_2O + \cdot OH \quad (2)$$

$$Fe^{3+} + e^- \rightarrow Fe^{2+} \quad (3)$$

To expand the application, the heterogeneous electro-Fenton (hetero-EF) has been developed with solid catalyst dosage or modified cathode replacing the dissolved Fe^{2+}, which could recover the metal ion, thus greatly reducing the sludge production and using over a wide pH range. Up to now, iron-based catalysts such as zero-valent iron (ZVI) (Martone et al., 2022), pyrite (Labiadh et al., 2015), chalcopyrite (Barhoumi et al., 2017), $Fe@Fe_2O_3$-CeO_2 composite (Zhang et al., 2022), core-shell FeCu@PC (Du et al., 2021) have been applied in hetero-EF. And with the activation of iron-based solid catalysts, it is effective under neutral and even alkaline conditions realizing the recovery of catalyst simultaneously. Besides, the bimetallic particles loaded carbon material modified cathode even metal-free carbon cathode such as 3D-MoO_2-porous biochar (PBC) (Zhang et al., 2021), MnxCo$_3$-x@C modified graphite felt (Huang et al., 2022), CuCo-O@ CNTs/NF (Zou et al., 2022), and ordered mesoporous carbon (OMC) (Tan et al., 2023) have been also reported to be applied to enhance the electron transport and reduce the metal ion leaching in hetero-EF. The carbon materials play an important role in generation of H_2O_2 on the cathode in the hetero-EF owing to the excellent performance of conductivity and ORR catalytic activity. Besides the metal-based particles can effectively activate H_2O_2 to •OH and achieve generation through the redox reaction and metal synergy on the cathode. In our previews study (Zhou et al., 2020b), Mn/Fe@ porous carbon (PC) was obtained with the Mn-doped MIL-53(Fe) precursor as the sacrificial templates. The Mn/Fe@ PC was applied to the in- situ generation and activation of H_2O_2 in hetero-EF system for TCS degradation. It showed great properties in wide pH range and high stability with low leaching of iron and manganese even in acid condition.

However, the preparation of the modified electrodes usually requires a binder with strong binding effect to load the catalyst onto the electrode skeleton, and it might block the reaction sites ultimately reducing the overall electrocatalytic performance in hetero-EF process (Qi et al., 2023). Therefore, the development of electrocatalysts with high catalytic activity and high stability directly grown on the surface of matrix materials without a binder exhibits great potential for the development of in situ hetero-EF processes. Zou (Zou et al., 2022) successfully prepared a CuCo-O@CNTs/nickel foam (NF) electrode without any adhesive and used in the hetero-EF system for in-situ degradation of sulfamethoxazole in a wide near-neutral pH range (5.6-9.0). Recently, the magnetically assembled electrode (MAE) with tuneable and modular electrode format has attracted much more attention. The MAE has the unique structures of a main electrode modified with 3D magnetic particles tightly bound to the 2D plate under the magnetic field. And the MAE has been applied in many fields such as detection (Zhang et al., 2022; Wei et al., 2023), electrochemical oxidation (Shao et al., 2022; Zhang et al., 2022) and peroxi-coagulation (Rao et al., 2022). It has been reported that the MAE can exactly enhance the effective catalytic area and the electrode stability, which makes it possible to recycle MAE providing a new idea for the preparation of modified cathode in hetero-EF system. Besides, to improve the stability of composite nanoparticles, carbon material-coupling iron oxide @noble metal particles has attracted attention (Zhang et al., 2019). And owing to the high activity and excellent catalytic performance in oxidation and reduction reactions, ruthenium (Ru) catalysts have attracted much attention in organic pollutant degradation (Qiu et al., 2021, 2022; Dai et al., 2023).

Herein, in this research, we synthesized the Ru@Fe_3O_4/rGO magnetic nanoparticles and assembled the innovative magnetically assembled cathode without any bonding agent. The magnetically assembled electrode (MAE) could not only avoid blocking the active sites of the catalyst, but also enhance the electron transportation owing to the synergy between Ru and Fe. And then the hetero-EF system was established with the assembled cathodes for degradation of DCF in different conditions for the investigation of the properties and the reusability. Moreover, the possible degradation mechanism was explored through quenching experiments and a possible degradation pathway of DCF was proposed. This work is expected to provide useful information for the preparation of modified electrode and degradation of organic pollutant in the wastewater for hydroxyl radical based EF process.

2. Materials and methods

2.1 Materials

Diclofenac (DCF, CAS: 15307-79-6, 90%) was purchased from Sigma-Aldrich. $FeCl_3\ 6H_2O$ (CAS: 10025-77-1, 98%), $FeCl_2 \cdot 4H_2O$ (CAS:7758-94-3, 98%), Na_2SO_4 (CAS: 7757-82-6, 99%), $RuCl_3$ (CAS: 10049-08-8, 98%) were purchased from Sigma, USA. Chromatographic pure acetonitrile and methanol were obtained from Merch (Darmstadt, Germany). Chromatographic pure acetic acid was bought from Komeo (Guangdong) Co., Ltd. Isopropanol (IPA, CAS: 67-63-0, 99.5%), furfuryl alcohol (FFA, CAS: 98-00-0, 98%), *p*-benzoquinone (BQ, CAS: 106-51-4, 99%), catalase (CAT, CAS: 9001-05-2, 3500 U/mg), L-histidine (CAS: 71-00-1, 99%) were supplied by Macklin (Shanghai, China). All the chemicals of analytical grade were used as received, and deionized water was used for the all solution in this work. Carbon paper was purchased from Shanghai Hesen CO., Ltd.

2.2 Preparation of Ru@Fe_3O_4/rGO catalyst and MAE electrode

Ru@Fe_3O_4/rGO catalyst was synthesized by solvothermal method referring to previous research with some improvements (Zhang et al., 2017; Zhang et al., 2019; Shen et al., 2023). The graphene oxide (GO) was synthesized with commercial graphite powder in accordance to modified Hummer's method reported in the literature (William S. Hummers et al., 1958). Then $FeCl_3$ $6H_2O$ (540 mg) and $FeCl_2 \cdot 4H_2O$ (200 mg) with a molar ratio of 2:1 and 100 mg GO were dissolved in 600 ml of deionized water and 40 mL polyethylene glycol was added to the well-mixed and distributed solution under sonication for 15 min. The pH value was adjusted to about 12 by adding ammonium hydroxide drop by drop and stirred at 60℃ for 2 h. Then the Fe_3O_4/GO was acquired and washed with deionized water, dried at 60℃ in the oven, and stored in a sealed container for used. 400 mg Fe_3O_4/GO and 41 mg $RuCl_3$ dispersed in 10 mL deionized water were moved into a four-neck flask. 15 mL of $NaBH_4$ solution in a constant pressure funnel was then added to the mixture slowly. After 60 min of reaction, the powders were washed with deionized water, and dried at 60℃ called Ru@Fe_3O_4/rGO. Fe_3O_4, Fe_3O_4/rGO, and Ru@Fe_3O_4 were fabricated with the same method expect without the additional of $RuCl_3$ and GO, $RuCl_3$, GO, respectively, as shown in Supporting Information (SI).

When Ru@Fe_3O_4/rGO catalysts were finally prepared, a permanent magnet was fixed at the back of the carbon paper. Then 20 mg of the magnetic Ru@Fe_3O_4/rGO dispersing in water would be attracted, fixed and supported on the other side of the carbon paper by invisible magnetic forces. The effective carbon paper area with Ru@Fe_3O_4/rGO adherence was about 9 cm^2. For comparison, Fe_3O_4, Fe_3O_4/rGO, Ru@Fe_3O_4, catalysts were also used to prepare the MAE electrodes to examine the degradation performance of DCF.

2.3 Characterizations and eletrochemical properties

The morphology of Ru@Fe_3O_4/rGO were characterized by scanning electron microscopy (SEM, Zeiss, Germany) equipped with an energy-dispersive spectroscopy (EDS) and transmission electron microscopy (TEM). The structure characteristics of Ru@Fe_3O_4/rGO were analysed by X-ray powder diffractometer (Panalytical Empyrean XRD, Netherlands) with Cu Kα radiation. X-ray photoelectron spectroscopy (XPS) was conducted for the investigation of metal valance. N_2 adsorption isotherm was used to determine the specific surface area and pore data of the AEs by a BET analyser (ASAP2460, Micromeritics, USA). The magnetic property of Ru@Fe_3O_4/rGO was tested by a vibrating sample magnetometer (VSM, Lakeshore-7404, USA).

The electrochemical property of catalysts was performed with an electrochemical workstation (CHI 760E, Chenhua Instruments, Inc., China) equipped with catalysts-coated glassy carbon electrode (GCE), Pt wire and saturated calomel electrode (SCE). The oxygen reduction performance was recorded by cyclic voltammetry (CV) in O_2/N_2–saturated 0.1 M Na_2SO_4 solution at pH=5 with a scan rate of 0.1 V s^{-1} from 0.2 to -0.8 V. The electrochemical impedance spectroscopy (EIS) analyses were performed in the frequency range of 100000 ~ 1 Hz. The electroactive surface area (EASA) of the catalysts was estimated by CV tests in the solution of 10 mM potassium ferricyanide containing 0.1 M KCl with Randles-Sevcik formula (**Eq.** (4)).

$$i_P = 2.69 \times 10^5 n^{\frac{3}{2}} A C D^{\frac{1}{2}} v^{\frac{1}{2}} \tag{4}$$

where i_P, n, A, C, D, v is the peak current (A), number of electrons, electroactive surface area (cm^2), concentration of the reactant (mol cm^{-3}), diffusion coefficient of the reactant (cm^2 s^{-1}) and scan rate (V s^{-1}), respectively.

2.4 Degradation experiments

The degradation experiments were performed in home-made quadrate single glass cell of 160 mL with 100 mL Na_2SO_4 solution containing 10 mg L^{-1} DCF with air continuously sparged. The prepared magnetically assembled electrode was performed as cathode with the exposed geometric area of 9 cm^2, and graphite electrode was used as anode with electrode spacing of 3 cm. The current was supplied by DC power (PS-302 DM, 0-30 V, 0-2 A) in the E-Fenton system. At each set time interval, 1.0 mL solution was sampled and analyzed immediately with filtration by 0.22-μm glass fiber membrane. For the determination of the active species during the DCF degradation, isopropanol (IPA), 1,4-benzoquinone (BQ), furfuryl alcohol (FFA), L- histidine and catalase (CAT) were added to the solution as •OH, $HO_2^{\bullet}/O_2^{\bullet-}$, $^1O_2$ and H_2O_2 trapping agents, respectively.

2.5 Analytical methods

A high-performance liquid chromatograph (HPLC, Waters 2695) was applied to detect the concentration of DCF. The 1% glacial acetic acid and acetonitrile (30:70, V/V) was as mobile phase at a flow rate of 1 mL min^{-1} with column temperature of 30 ± 1.0 ℃ at 276 nm. The total organic carbon (TOC) was analyzed with the TOC analyzer (LiquiTOC trace, Elementar, Germany). The intermediate products of DCF degradation were determined using ultra-performance liquid chromatography coupled with orbitrap mass spectrometry (UPLC-MS/MS, model Q-Exactiveplus, Thermo Fisher Technology Co., Ltd., USA). The Electron Paramagnetic Resonance (EPR) spectra were measured by Bruker EMX plus instrument

(Germany) with 5,5-dimethyl-1-pyrroline N-oxide (DMPO) and 2,2,6,6-tetramethyl-4-piperidone (TEMP) for trapping •OH and $O_2^{\bullet-}$ respectively. The dissolved metal ions were detected by an Inductively coupled plasma atomic emission spectrometry (ICP-AES, iCAP-6000, Thermo, USA). The samples were first filtered by glass fiber filter membrane (pore size of 0.22 μm), then injected into the apparatus.

3. Results and discussion

3.1 Morphology and structure characteristics

The surface morphology and microstructure characteristics of as-obtained products Ru@Fe_3O_4/rGO were determined by scanning electron microscope (SEM) and transmission electron microscopy (TEM). As shown in **Fig.1a-d,** the SEM and TEM images showed that spherical nanoparticles morphology of the composite had a uniform size and the dispersed nanoparticles anchored on the rGO nanosheets substrates in Ru@Fe_3O_4/rGO. High resolution transmission electron microscopy (HR-TEM) images are displayed in **Fig.1e**. Corresponding lattice space of Fe_3O_4 and Ru were also detected in HR-TEM and the lattice spacings assigned to 0.198 nm and 0.238 nm were matched perfectly with the (311) and (400) planes of Fe_3O_4, respectively. Besides, the lattice spacing of 0.23 nm was assigned to the (100) plane of Ru. And the energy-dispersive spectroscopy (EDS) mapping illustrated in **Fig.1f** showed that Ru, C, Fe and O were distributed homogeneously throughout the architecture proving the existence of those elements in the nanocomposites and the successful synthesis of the composite nanomaterials.

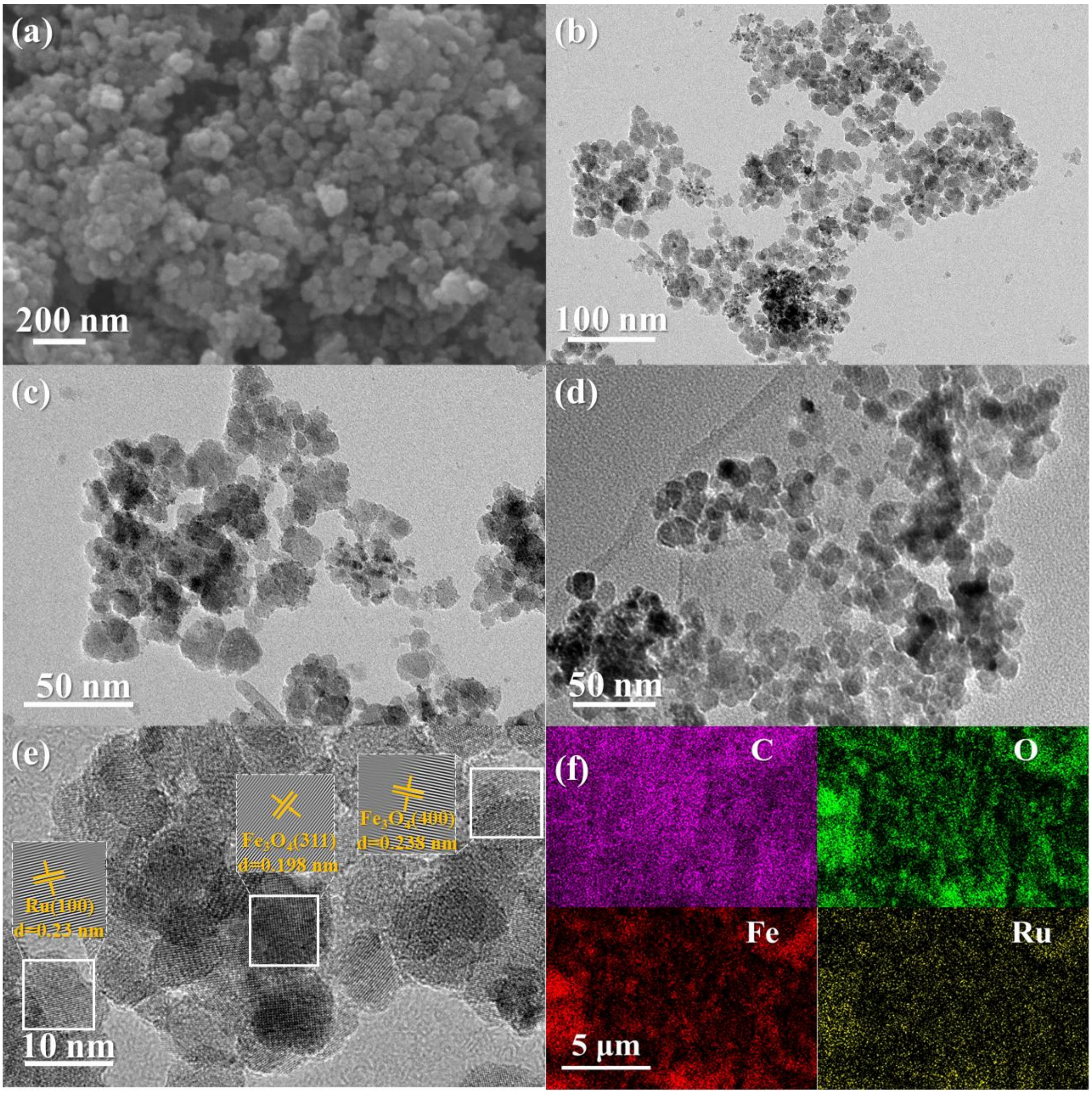

Fig. 1 SEM images (a), TEM images (b-d), HR-TEM (e) and EDS elemental mapping (f) of Ru@Fe_3O_4/rGO.

The XRD pattern was performed to analyze the crystal structures of the catalysts and presented in **Fig.2a**. All the samples of Fe_3O_4, Fe_3O_4/rGO, Ru@Fe_3O_4 and Ru@Fe_3O_4/rGO presented the characteristic peaks of Fe_3O_4 located at 30.1 ° (220), 35.6 ° (311), 43.3 ° (400), 53.7 ° (422), 57.4 ° (511) and 62.8 ° (440), which was consistent with the Fe_3O_4 standard card (PDF#89–0688). No others characteristic peaks of impurities and no obvious diffraction peaks corresponding to the carbon in Fe_3O_4/rGO, Ru@Fe_3O_4 and Ru@Fe_3O_4/rGO were observed which suggested the good maintenance of the crystal structure. And there existed the characteristic peaks of rGO in Fe_3O_4/rGO and Ru@Fe_3O_4/rGO indicating the effectively reduce of GO into graphene (Liu et al., 2015). Besides compared with Fe_3O_4, no reflections owing to metallic ruthenium were observed in Ru@Fe_3O_4/rGO, which indicated that the Ru nanoparticles were uniformly dispersed with a very small particle size.

The full XPS spectrum of Ru@Fe_3O_4/rGO confirmed the existence of Fe, Ru and O elements as was shown in **Fig.S1**. As seen in **Fig.2b**, the deconvolution of Ru 3d spectra provides $3d_{5/2}$ and $3d_{3/2}$ peaks, the peaks centered at 286.3 eV and 281.3 eV were assigned to RuO_2, and the peaks centered at 284.3 eV and 280.2 eV were ascribed to Ru(III) and Ru^0, respectively, indicating the doping of the Ru element (Dai et al., 2023). The spectrum of Fe 2p could be fitted well with two spin-orbit at 711 eV and 724.5 eV corresponding to Fe $2p_{3/2}$ and Fe $2p_{1/2}$, besides, the peak at 718.4 eV was ascribed to the satellite peaks. And the peaks could be deconvolved into the Fe^{2+} peaks at 709.9 eV and Fe^{3+} peaks at 711 eV, 712.4eV, 714.4 eV and 731.8 eV, respectively (**Fig.2c**) suggesting the existence of Fe_3O_4 in Ru@Fe_3O_4/rGO which was in accordance with the result of XRD. In addition, the mixture valence of Fe and Ru species might provide rich reaction sites and enhance electron transfer by synergy. The O 1s spectra displayed in **Fig.2d** included several major peaks at 529.3 eV, 529.8 eV, 530.3 eV, 531.3 eV corresponding to lattice O (O_{lat}), oxygen vacancies (O_{vac}), oxygen in hydroxyl group (O_{OH}) and oxygen in H_2O, respectively (Shi et al., 2023).

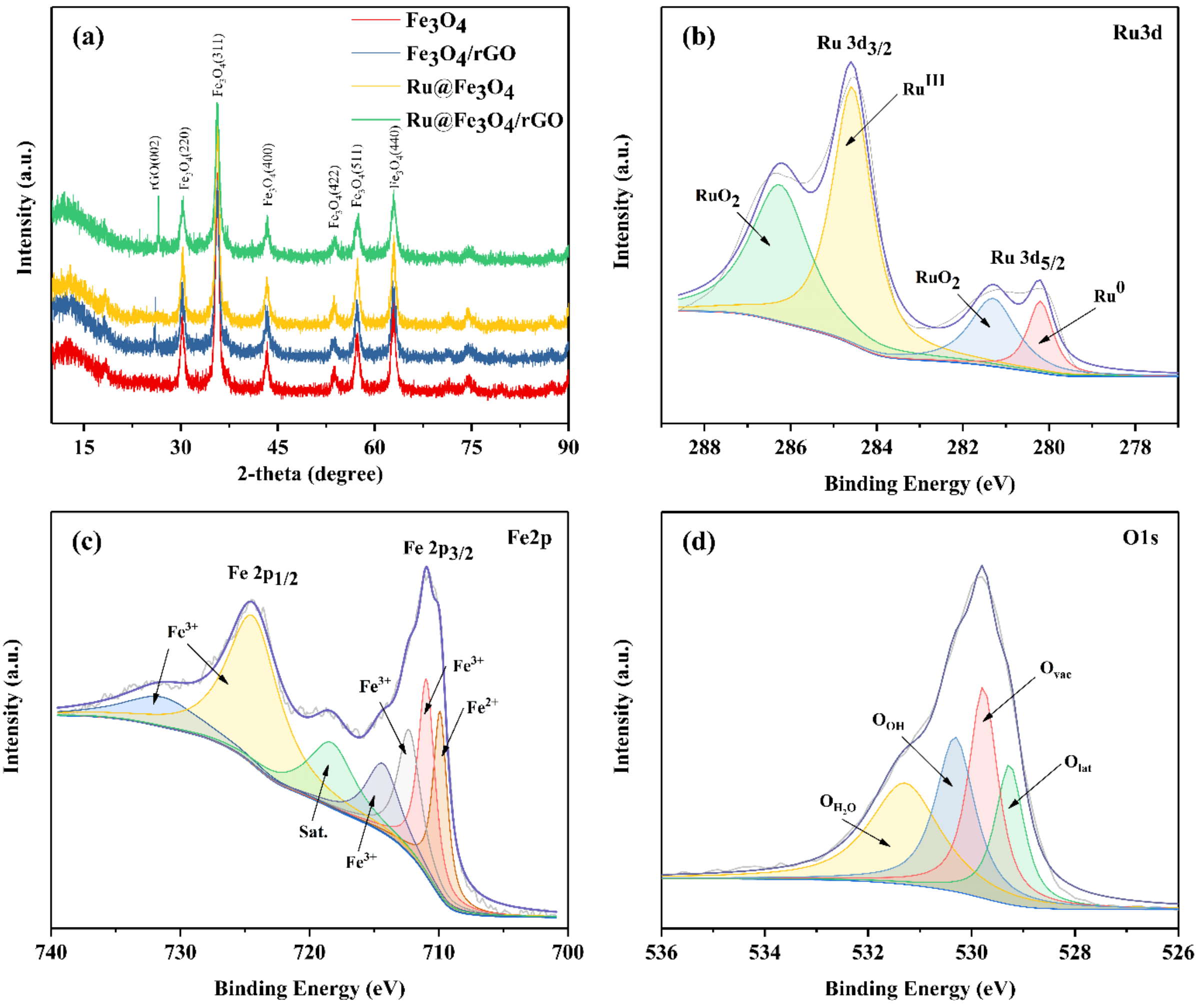

Fig. 2 The XRD patterns of different catalysts (a) and high-resolution scanning XPS spectra for Ru 3d (b), Fe 2p (c) and O 1s (d) of Ru@Fe_3O_4/rGO.

3.2 Electrochemical characterization

Electrochemical activity analysis was carried out to identify the ORR catalytic activity and electron transfer via cyclic voltammetry (CV) experiments and electrochemical impedance spectroscopy (EIS). As shown in **Fig.3a**, compared with Fe_3O_4 and Ru@Fe_3O_4, Fe_3O_4/rGO and Ru@Fe_3O_4/rGO showed higher response current intensity owing to the improvement of the electrical conductivity with the adding of rGO, which might provide abundant active sites for ORR to generate H_2O_2. Besides, it was obvious that there was oxygen reduction peak at -0.52 V vs. SCE under O_2-saturated while no oxygen reduction peak was observed in N_2-saturated, indicating the ORR catalytic performance of Ru@Fe_3O_4/rGO catalyst. Notably, all the samples existed two peaks at about 0.461 V vs. SCE and 0.34 V vs. SCE corresponding to the redox couples of $Fe^{II/III}$ suggesting the regeneration of Fe^{II} on cathode for continuous activation of generated H_2O_2. Compared with Fe_3O_4/rGO, Ru@Fe_3O_4/rGO showed higher current intensity owing to the doping of Ru which might enhance the electron transfer. Moreover, as displayed in **Fig. S2**, the electroactive surface area (EASA) of the catalysts was performed in 10 mM $K_3[Fe(CN)_6]$ solution with 1.0 M KCl as the supporting electrolyte. The peak current of Ru@Fe_3O_4/rGO electrode (0.267 V, 4.14×10^{-5} A) was much higher than Ru@Fe_3O_4 (0.267 V, 1.88×10^{-5} A), Fe_3O_4/rGO (0.248 V, 2.48×10^{-5} A) and Fe_3O_4 (0.266 V, 7.13×10^{-6} A). According to the Randles-Sevcik formula, the EASA of Ru@Fe_3O_4/rGO (0.061 cm^2) was 2.2 times of Ru@Fe_3O_4 (0.028 cm^2), 1.67 times of Fe_3O_4/rGO (0.037 cm^2) and 5.8 times of Fe_3O_4 (0.011 cm^2), respectively. For the CVs of Ru@Fe_3O_4/rGO catalyst under different scan rate, the linearly of the anodic peak current to the scan rate (R^2=0.999) was superior to that of the scan $rate^{1/2}$ (R^2=0.989), suggesting that the surface adsorption control process played a dominant role in Ru@Fe_3O_4/rGO electrode.

Additionally, the electrochemical impedance spectroscopy (EIS) was conducted to reveal the electron transfer of the catalysts (**Fig.3b**), Fe_3O_4/rGO and Ru@Fe_3O_4/rGO exhibited lower charge/mass-transfer resistance compared with Ru@Fe_3O_4 and Ru@Fe_3O_4 indicating that rGO could increase the electrical conductivity and enhance the electron transfer, which was in accord with the results of CV plots.

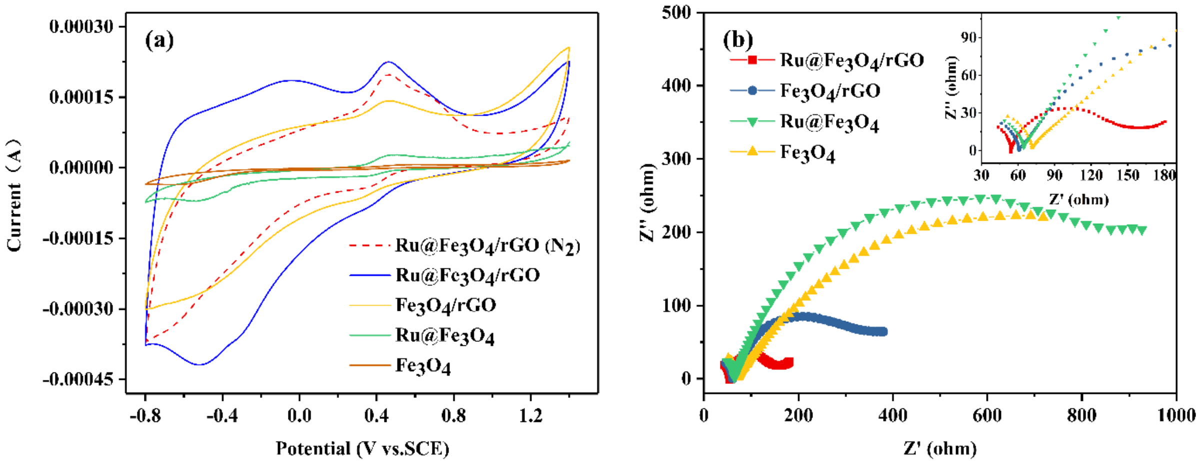

Fig. 3 CV curves with different modified electrodes in N_2-saturated (dotted line) and O_2-saturated (full line) (a) and EIS plots (b) in Na_2SO_4 solution.

3.3 DCF degradation in hetero-EF process

The degradation of DCF (10 mg L^{-1}) was evaluated in hetero-EF process by magnetically assembled cathodes and the results were showed in **Fig.4**. As displayed in **Fig. 4a,** consistently with the above electrochemical results, below 20% of DCF was removed in 120 min with the bare cathode without additional of magnetic nano-catalyst because of the less generation of H_2O_2 and activation to •OH. With Fe_3O_4 MAE, Fe_3O_4/rGO MAE, Ru@Fe_3O_4 MAE as the cathodes in hetero-EF process, the DCF removal efficiency increased to 66%, 72%, 73%, respectively, mainly due to the abundant 2e^- ORR catalytic active sites for H_2O_2 generation of rGO and the enhanced electron transfer between Ru and Fe for •OH generation. Thus, Ru@Fe_3O_4/rGO MAE reflected the best removal performance of DCF and the nearly 100% DCF was removed with Ru@Fe_3O_4/rGO MAE. Furthermore, to investigate the catalytic of the Ru@Fe_3O_4/rGO MAE hetero-EF process, DCF were measured under different conditions in **Fig.4b**. The adsorption of Ru@Fe_3O_4/rGO MAE could contribute 55% DCF removal in open circuit which might enhance the in-suit degradation on the cathode. And without the magnet to assemble MAE in hetero-EF process, DCF degradation efficiency increased to 86% mainly because of generation on the carbon paper cathode (Wang et al., 2013) and activation of H_2O_2 by Ru@Fe_3O_4/rGO. While with the in-situ generation and activation of H_2O_2 by Ru@Fe_3O_4/rGO MAE, the DCF degradation efficiency increased markedly further proving the ORR catalytic to generate H_2O_2 and activation of H_2O_2 of the MAE cathode.

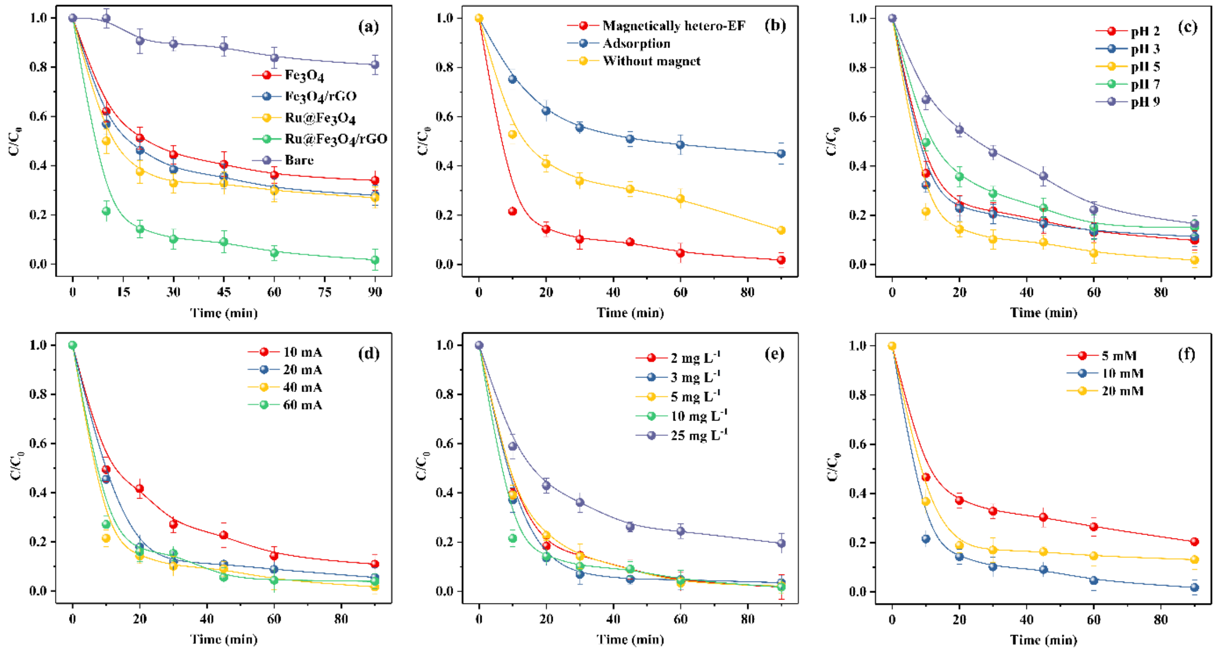

Fig. 4 DCF removal in magnetically hetero-EF process with different magnetically assembled cathodes (a); DCF removal with Ru@Fe_3O_4/rGO catalysts under different conditions (b-f). Unless otherwise stated, the reaction conditions are: pH=5, [DCF]= 10 mg L^{-1}, I= 40 mA, [Na_2SO_4] =10 mmol L^{-1}.

The effects of operating parameters on the DCF degradation including initial pH, current density, DCF concentration and electrolyte concentration were also investigated systematically. Generally, compared with the traditional E-Fenton process, hetero-EF process could greatly widen applied pH range significantly effecting the degradation efficiency of organic pollutants. As was shown in **Fig.4c**, with the Ru@Fe_3O_4/rGO MAE as cathode, the highest DCF removal efficiency about 100% within 90 min was obtained under pH 5, while removal efficiency sharply decreased to about 90% in the strong acid condition and about 85% in the neutral and alkaline conditions, respectively. Owing to the rapid decomposition of the generated H_2O_2 in alkaline conditions (**Eq.** (5)), the DCF degradation efficiency decreased to about 85% with the pH increased to 9. Note that the DCF removal efficiency under different pH conditions from 2-9 were more than 80% indicating the excellent E-Fenton performance of the Ru@Fe_3O_4/rGO MAE under a wide pH range. As shown in **Fig.4d**, the degradation efficiency of DCF increased with the increase of current from 10 mA to 40 mA attributed to the enhanced electron transfer for the generation and activation of H_2O_2. Whereas, the further increase of current might have a negative influence on DCF degradation owing to the occurrence of side reactions such as hydrogen evolution and water electrolysis. And the effect of initial DCF concentration was evaluated and shown in **Fig.4e**, nearly 100% DCF could be removed under the different concentration from 2 mg L^{-1} to 10 mg L^{-1} because of the rapidly adsorption and enrichment by the dispersed catalyst and then fixed magnetically on the cathode. With higher DCF concentration to 20 mg L^{-1}, DCF along with its degradation intermediates might occupy the active sites of the cathode and consume the reactive oxidation free radicals, and thus reduced the degradation efficiency. As displayed in **Fig.4f**, the electrolyte concentration was optimized to be 10 mM.

$$\mathrm{H_2O_2 + 2OH^- \rightarrow O_2 + 2H_2O + 2e^-} \qquad (5)$$

As shown in **Fig.5a**, the mineralization degree was reflected by the TOC removal efficiency during the DCF degradation in the Ru@Fe_3O_4/rGO MAE hetero-EF process. The DCF removal efficiency reached 78.4% in 10 min and 98.2% in 90 min, respectively, while the TOC removal efficiency just 11.64% and 49.3%, respectively, which was attributed to produce of the intermediate during DCF degradation. Besides, to explore the cyclic and reusability of the Ru@Fe_3O_4/rGO MAE, consecutive experiments were conducted and showed in **Fig.5b**, it could achieve as high as 95.5% in 60 min in the first cycle, and decreased to about 85% after 5 consecutive reusable experiments, proving the great stability and reusability of the Ru@Fe_3O_4/rGO MAE in the hetero-EF process. As shown in **Fig.5c**, in the 5 consecutive cycles, the concentration of the total dissolved Ru below 0.03 mg L^{-1} except the total dissolved Fe was acceptable using MAE modified with Ru@Fe_3O_4/rGO as cathode. The high concentration of the total dissolved Fe mainly came from the dissolution of Fe_3O_4. It can be deduced that, coating detachment (Ru@Fe_3O_4/rGO) from MAE may mainly contributed to MAE deactivation. In the 5 consecutive cycles, the total dissolve Fe concentration decreasing gradually, the total dissolved Ru concentration remaining at a low and stable level, and MAE keeping high DCF degradation performance, indicated the favorable stability of MAE.

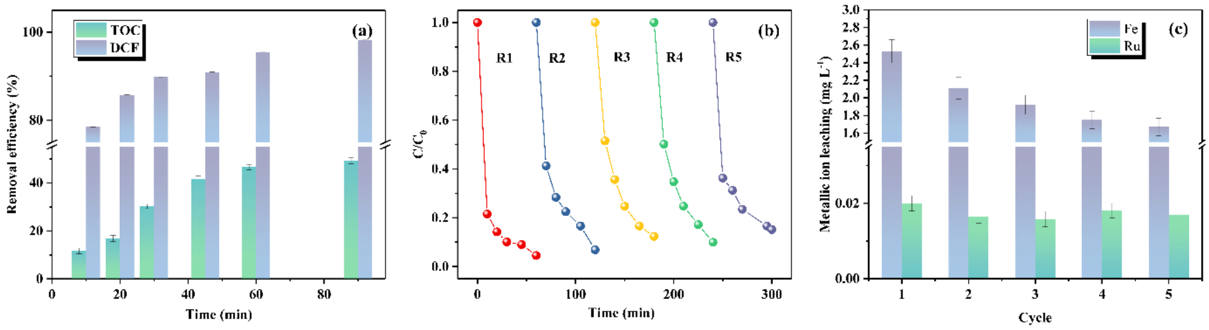

Fig.5 TOC removal efficiency with Ru@Fe_3O_4/rGO MAE (a), stability evaluation (b) and metallic ion leaching (c) with five continual cycles.

Besides, the N_2 adsorption-desorption curves of Ru@Fe_3O_4/rGO samples before reaction and after reaction were performed in **Fig.6a** to analyse the surface area and pore size distribution. The N_2 adsorption-desorption isotherm of Ru@Fe_3O_4/rGO is a type IV adsorption–desorption curve with H3 hysteretic loops indicating the mesoporous structure of Ru@Fe_3O_4/rGO. And the average pore diameter (Average pore diameter calculated by the desorption data using Barrett–Joyner–Halenda (BJH) method), Brunauer-Emmett-Teller (BET) surface areas and total pore volume of the fresh catalyst were 16 nm, 125.8 m^2 g^{-1} and 0.38 cm^3 g^{-1}, respectively. Compared with the fresh sample, the BET surface areas and total pore volume of the fresh catalyst decreased slightly to 74.36 m^2 g^{-1}, and 0.357 cm^3 g^{-1}, respectively, while the average pore diameter increased slightly to 23 nm after reaction. With the degradation of DCF, the intermediate products might occupy the active site affecting the degradation efficiency. As shown in **Fig.6b**, vibrating sample magnetometer (VSM) with a 20000 Oe magnetic field was used for studying the magnetic properties of Ru@Fe_3O_4/rGO after reaction. According to the VSM results, the saturation magnetization (Ms) values of fresh sample was 0.328 emu g^{-1}, while the used sample decreased slightly to 0.266 emu g^{-1}, indicating the ferromagnetism of the catalysts making it possible for the self-assembly, collection and recycle of electrodes.

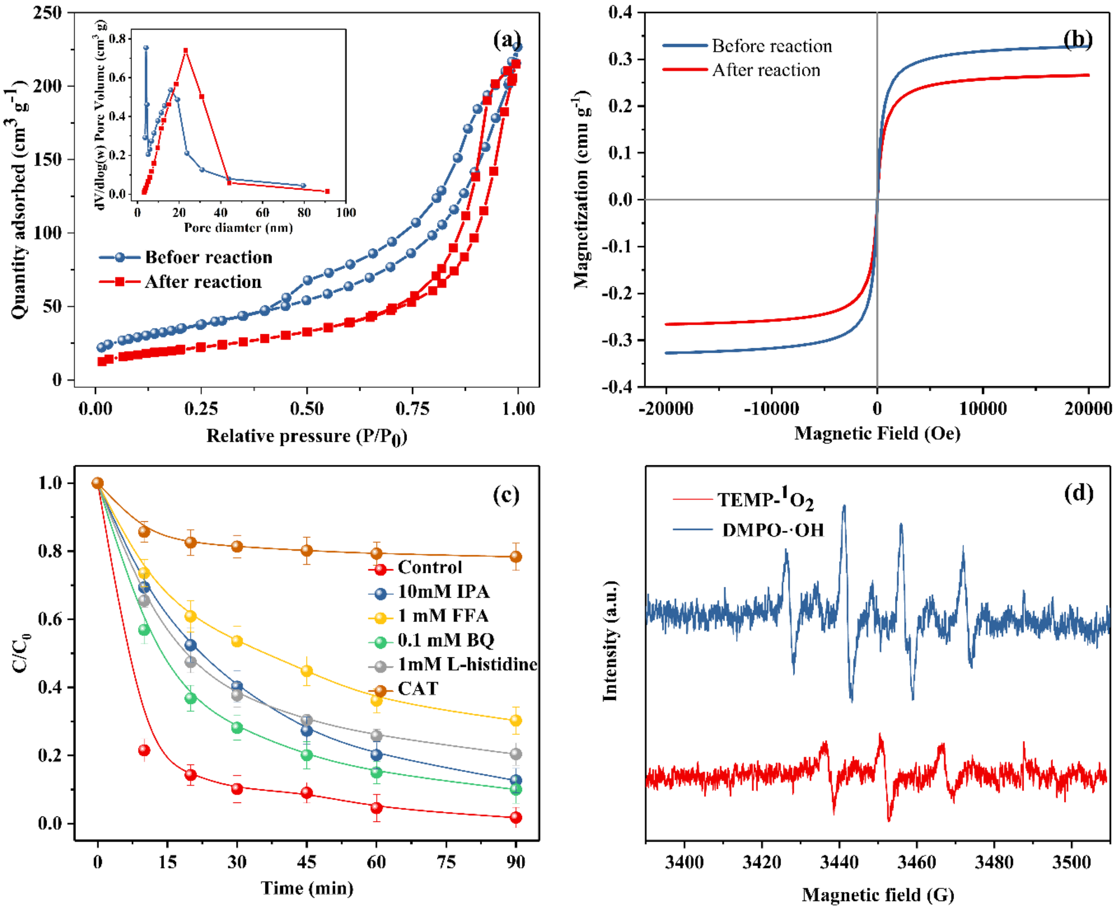

Fig. 6 N_2 adsorption isotherms and pore size distribution (a) and the magnetic hysteresis loops of fresh and used Ru@Fe_3O_4/rGO. DCF degradation in Ru@Fe_3O_4/rGO MAE hetero-EF process with excessive scavengers (c) and EPR spectra with TEMP and DMPO as spin-trapping agents (d) in Ru@Fe_3O_4/rGO MAE

hetero-EF process.

3.4 Proposed catalytic mechanism

To determine the potential reactive oxygen species (ROSs) involved in Ru@Fe_3O_4/rGO MAE hetero-EF process, scavenging experiments were conducted using isopropanol (IPA) to quench •OH, furfuryl alcohol (FFA) and L-histidine to quench $^1O_2$, catalase (CAT) to quench H_2O_2 and p-benzoquinone (BQ) to quench $HO_2^{\bullet}$/ $O_2^{\bullet -}$. Notably, as displayed in **Fig.6c**, compared with the DCF removal efficiency without scavenger, the scavengers showed significant inhibition with lower DCF removal efficiency following the order: no scavenger (98.2%)>BQ(90%)>IPA(87.4%)> L-histidine (79.6%)>FFA(69.7%)>CAT(21.7%), implying that the involvement of $HO_2^{\bullet}$/ $O_2^{\bullet -}$, •OH , $^1O_2$ and H_2O_2. Obviously, the most significant inhibition of DCF degradation was obtained with CAT indicating that the generation of the reactive oxygen species (ROS) was mainly attributed to the activation of H_2O_2 by Ru@Fe_3O_4/rGO catalyst. Meanwhile, with the addition of FFA, L-histidine, IPA and BQ, DCF removal efficiency decreased to 69.7%, 79.6%, 87.4% and 90%, respectively, confirming the $^1O_2$ was the main ROS participating and •OH, $HO_2^{\bullet}$/ $O_2^{\bullet -}$ were the other important key factors in DCF degradation. To further conform the exist of ROS in this process, EPR tests were conducted with DMPO and TEMP as trapping agent and shown in **Fig.6d**. The obviously four-fold typical peak with the intensity ratio of 1:2:2:1 assigned to the DMPO- •OH signal suggesting the generation of •OH in the Ru@Fe_3O_4/rGO MAE hetero-EF process. Besides, the triple signal of 1:1:1 was the typical peak of TEMP-$^1O_2$ indicating the involvement of $^1O_2$ in this process. The results of EPR were in line with the DCF degradation experiment further confirming the existence and involvement of the ROS in Ru@Fe_3O_4/rGO MAE hetero-EF process for DCF degradation.

Based on above analyses, the proposed catalytic mechanism of DCF degradation in Ru@Fe_3O_4/rGO MAE hetero-EF process was proposed in **Fig.7**. In the first step, the oxygen molecules diffused into the electrolyte and adsorbed on the surface reactive sites of Ru@Fe_3O_4/rGO MAE. And then the adsorbed O_2 was in-situ reduced to $HO_2^{\bullet}$/ $O_2^{\bullet-}$ (**Eqs.** (6)-(7)) via one-electron ORR pathway and reduced to H_2O_2 via another one-electron pathway of $HO_2^{\bullet}$/ $O_2^{\bullet-}$ (**Eqs.** (8)) or 2e^- ORR pathway (**Eqs.** (9)). Besides, the excessive $HO_2^{\bullet}$/ $O_2^{\bullet-}$ in the solution could also generate $^1O_2$ through the reaction of $HO_2^{\bullet}$/ $O_2^{\bullet-}$ (**Eqs.** (10)-(11)) (Li et al., 2023; Ye et al., 2023). Subsequently, the •OH was generated with the in-situ activation of H_2O_2 under the synergistic effect of the Fe and Ru according to previous study (**Eqs.** (12)-(14)) (Rokhina et al., 2009). Besides, as reported in previews study (Pan et al., 2021), the RuO_2 could also be an active site for the activation of H_2O_2 in the heterogeneous Fenton-like system. In addition, the generated $\equiv Fe^{III}$ could be reduced on the cathode (**Eq.** (15)) which remarkably improved the regeneration of $\equiv Fe^{II}$ to active H_2O_2 persistently. What could not be ignored was that the existence of Ru^0 was the main reason for the production of active hydrogen [H] to reduce DCF (**Eqs.** (16)-(17)), which reduced the electron cloud density of DCF and further accelerated the advanced oxidative degradation of DCF. Finally, with the corporate effects of various ROS generated in the Ru@Fe_3O_4/rGO MAE hetero-EF process, DCF could be attacked and mineralized into CO_2 and H_2O.

$$O_2 + e^- \rightarrow O_2^{\bullet-} \quad (6)$$

$$O_2^{\bullet-} + H^+ \rightarrow HO_2^{\bullet} \quad (7)$$

$$O_2^{\bullet-} + 2H^+ + e^- \rightarrow H_2O_2 \quad (8)$$

$$O_2 + 2H^+ + 2e^- \rightarrow H_2O_2 \quad (9)$$

$$2\mathrm{O}_2^{\cdot-} + 2\mathrm{H}^+ \rightarrow \mathrm{H}_2\mathrm{O}_2 + {}^1\mathrm{O}_2 \tag{10}$$

$$\mathrm{HO}_2^{\cdot} + \mathrm{O}_2^{\cdot-} \rightarrow {}^1\mathrm{O}_2 + \mathrm{HO}_2^- \tag{11}$$

$$\equiv \mathrm{Fe}^{\mathrm{II}} + \mathrm{H}_2\mathrm{O}_2 \rightarrow \equiv \mathrm{Fe}^{\mathrm{III}} + \cdot\mathrm{OH} + \mathrm{OH}^- \tag{12}$$

$$\equiv \mathrm{Ru}^{\mathrm{III}} + \mathrm{H}_2\mathrm{O}_2 \rightarrow \equiv \mathrm{Ru(OOH)}^{\mathrm{II}} + \mathrm{H}^+ \rightarrow \equiv \mathrm{Ru}^{\mathrm{II}} + \mathrm{HO}_2 + \mathrm{H}^+ \tag{13}$$

$$\equiv \mathrm{Ru}^{\mathrm{II}} + \mathrm{H}_2\mathrm{O}_2 \rightarrow \equiv \mathrm{Ru}^{\mathrm{III}} + \cdot\mathrm{OH} + \mathrm{OH}^- \tag{14}$$

$$\equiv \mathrm{Fe}^{\mathrm{III}} + \mathrm{e}^- \rightarrow \equiv \mathrm{Fe}^{\mathrm{II}} \tag{15}$$

$$\mathrm{Ru}^0 + \mathrm{H}^+ + \mathrm{e}^- \rightarrow \mathrm{Ru}^0 \cdot [\mathrm{H}] \tag{16}$$

$$\mathrm{Ru}^0 \cdot 2[\mathrm{H}] + [\mathrm{C}_{14}\mathrm{H}_{10}\mathrm{Cl}_2\mathrm{NO}_2]^- \rightarrow \mathrm{Ru}^0 + 2\mathrm{Cl}^- + [\mathrm{C}_{14}\mathrm{H}_{12}\mathrm{NO}_2]^- \tag{17}$$

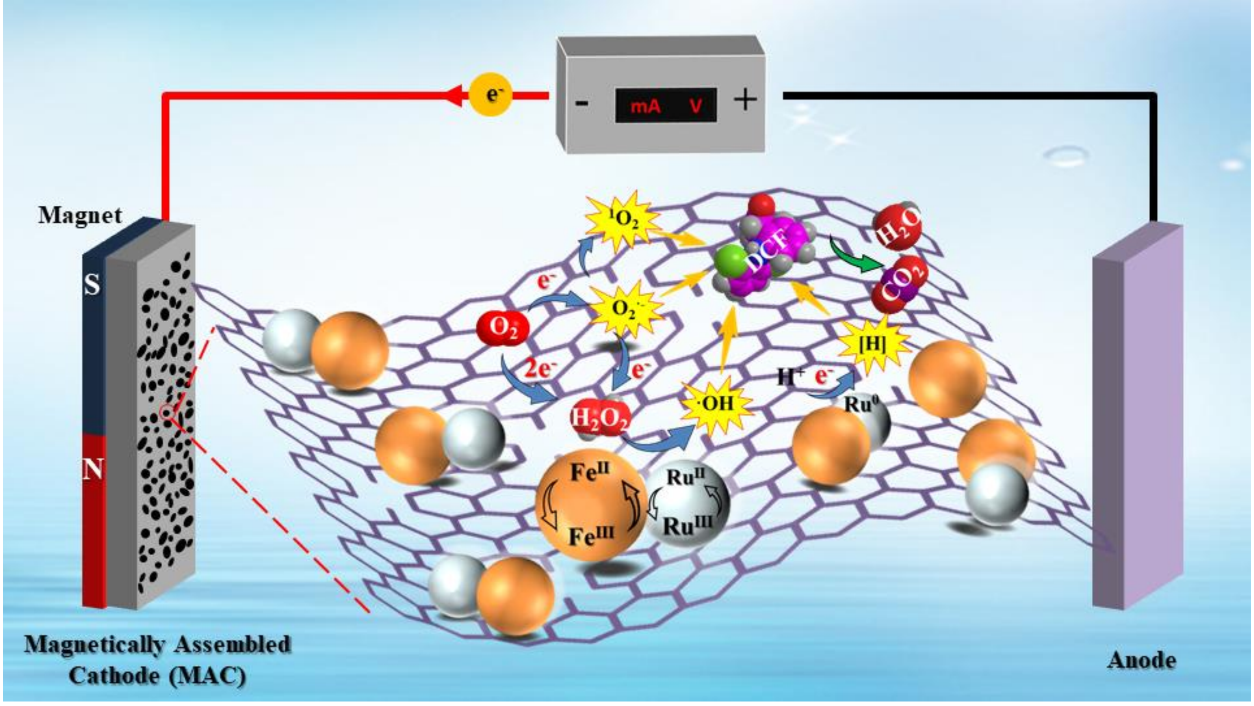

Fig. 7 Schematic diagram of the DCF degradation mechanism in Ru@Fe_3O_4/rGO MAE hetero-EF process.

3.5 Proposed degradation pathway and toxicity evaluation of DCF

The intermediates of DCF degradation in Ru@Fe_3O_4/rGO MAE hetero-EF process were measured and analyzed by LC-MS/MS and 11 compounds were deduced named from IP1-IP11 (Table **S1**). Based on the molecular structure of products and previous research of DCF degradation, three possible pathways were proposed and shown in **Fig.8** mainly including dechlorination, hydroxylation and ring opening. In the first pathway, DCF was attacked by [H] to dechlorinate to form IP1 or IP2, and further dechlorination was followed to converting into IP3 or IP4, respectively. Then IP3 and IP4 were degraded with hydroxylation (IP5) and ring opening process (IP6). In the second pathway, with the synchronization dechlorination and hydroxylation process, hydroxyl substituted chlorine and DCF was firstly converted to IP7 and then further form IP8 with hydroxylation process. In the third pathway, the hydroxyl was firstly added to the piperazine ring via the hydroxylation reaction to form IP9 and IP10 and further converted to IP11. Based on the previous reaction including hydroxylation and dechlorination reaction, the intermediates (IP6, IP8, and IP11) were further oxidized by the ROS and converted to inorganic substances, such as CO_2, H_2O, Cl^- and NO_3^-.

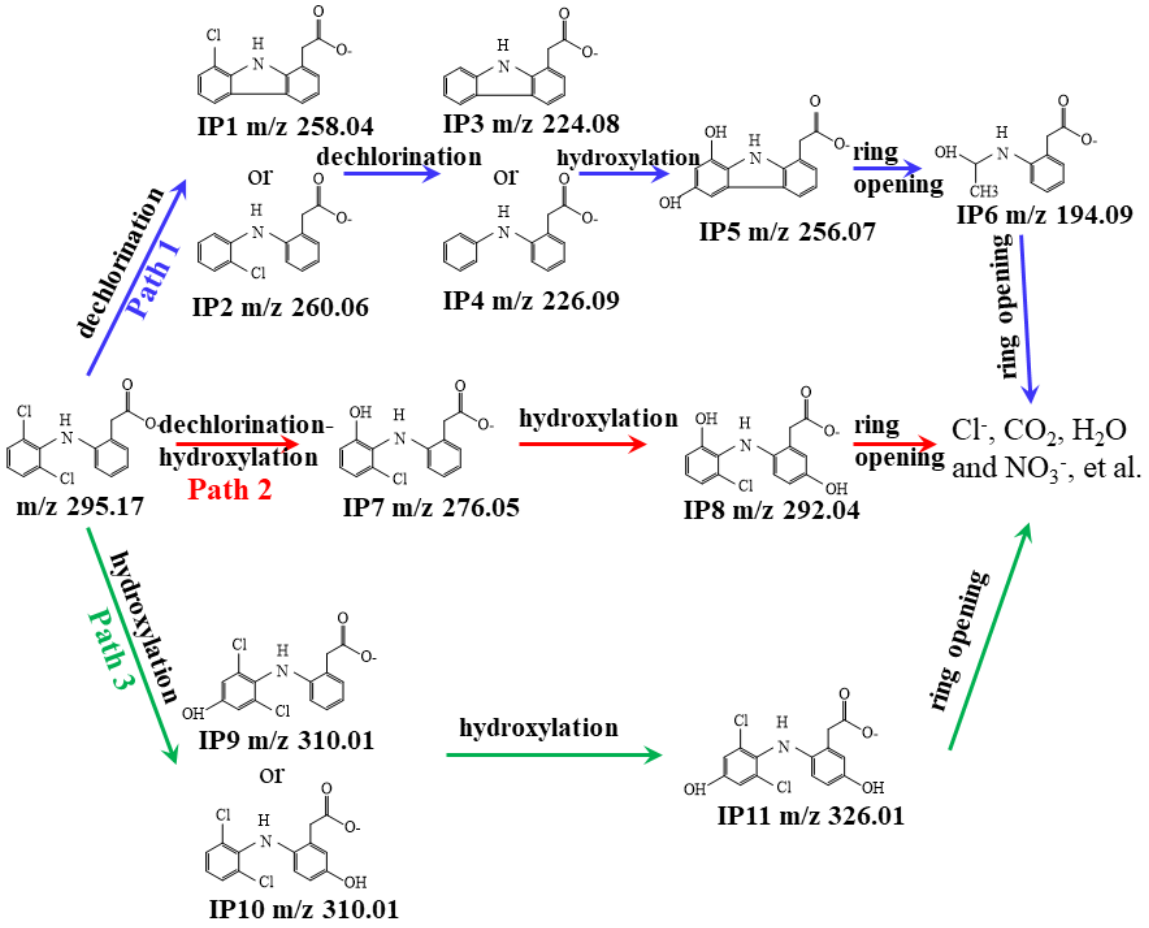

Fig. 8 The possible pathway of DCF degradation in Ru@Fe_3O_4/rGO MAE hetero-EF process.

The toxicity of DCF and intermediates of the degradation in Ru@Fe_3O_4/rGO MAE hetero-EF process was evaluated by the ECOSAR program. As shown in **Fig.S3**, the LC50 of DCF to fish, daphnia and green algae was all in the range of 10-100 mg L^{-1} indicating the acute toxicity of DCF was in the category of harmful, while the LC50 of intermediates to fish, daphnia and green algae was all higher than that of DCF indicating that the acute toxicity was significantly reduced with the degradation of DCF. And similar results can be obtained for the chronic toxicity evolution. The Chv of DCF to fish, daphnia and green algae was in the range of 1-10 mg L^{-1}, 1-10 mg L^{-1} and 10-100 mg L^{-1}, respectively, and the chronic toxicity of DCF was in the category of toxic to fish and daphnia and harmful to green algae. The Chv of intermediates was significantly higher than DCF with lower chronic toxicity. Thus, the ecological risk of DCF degradation in Ru@Fe_3O_4/rGO MAE hetero-EF process was significant reduced promising for the future practical application of the electrochemical treatment for DCF degradation.

4. Conclusion

In this study, the Ru@Fe_3O_4/rGO nanocomposite catalyst has been successfully synthesized and attracted to assemble as cathode by magnetic force for degradation of DCF in heterogeneous E-Fenton process. The synthesized Ru@Fe_3O_4/rGO with higher electroactive surface area and electron transfer could provide abundant reactive sites for ORR to generate and activate H_2O_2. With the quick adsorption and catalytic, Ru@Fe_3O_4/rGO MAE exhibited a superior electrochemical activity and high stability in wide conditions for DCF degradation. Based on the quenching experiments and EPR test, $^1O_2$ and •OH were the main ROS involved in the Ru@Fe_3O_4/rGO MAE hetero-EF process. With the catalytic of Ru@Fe_3O_4/rGO, adsorbed O_2 was in-situ reduced via one-electron ORR or $2e^-$ ORR pathway, and then further generate $^1O_2$ or active to •OH with the synergistic effect of the Fe and Ru. In addition, DCF was degraded to less toxic intermediates by the attack of ROS with three possible pathways including dechlorination, hydroxylation and ring opening. This work provides new insights into the assembly of electrode and displays a new practical application prospect of the materials for high-efficient removal and degradation of persistent organic pollutant from wastewater.

Acknowledgements

This work was supported by the National Natural Science Foundation of China (U21A20290, 22176044, 22006024, 82001957), Guangdong Basic and Applied Basic Research Foundation (2022A1515011656), Projects of Talents Recruitment of GDUPT (RC-XJ2022000501), and Maoming science and Technology Project (2023386).

References

Barhoumi, N., Olvera-Vargas, H., Oturan, N., Huguenot, D., Gadri, A., Ammar, S., Brillas, E., Oturan, M.A., 2017. Kinetics of oxidative degradation/mineralization pathways of the antibiotic tetracycline by the novel heterogeneous electro-Fenton process with solid catalyst chalcopyrite. Applied Catalysis B: Environmental 209, 637-647.

Dai, C., You, X., Liu, Q., Han, Y., Duan, Y., Hu, J., Li, J., Li, Z., Zhou, L., Zhang, Y., Liu, S., 2023. Peroxymonosulfate activation by Ru/CeO_2 for degradation of Triclosan: Efficacy, mechanisms and applicability in groundwater. Chemical Engineering Journal 463, 142479.

Du, X., Fu, W., Su, P., Su, L., Zhang, Q., Cai, J., Zhou, M., 2021. Trace FeCu@PC Derived from MOFs for Ultraefficient Heterogeneous Electro-Fenton Process: Enhanced Electron Transfer and Bimetallic Synergy. ACS ES&T Engineering 1, 1311-1322.

Dung Nguyen, M., Binh Nguyen, T., Hai Tran, L., Giang Nguyen, T., Fatimah, I., Prasetyo Kuncoro, E., Doong, R., 2023. Z-scheme S, B co-doped g-C_3N_4 nanotube@MnO_2 heterojunction with visible-light-responsive for enhanced photodegradation of diclofenac by peroxymonosulfate activation. Chemical Engineering Journal 452, 139249.

Huang, S., Wang, Y., Qiu, S., Wan, J., Ma, Y., Yan, Z., Xie, Q., 2022. In-situ fabrication from MOFs derived MnxCo_3-x@C modified graphite felt cathode for efficient electro-Fenton degradation of ciprofloxacin. Applied Surface Science 586, 152804.

Labiadh, L., Oturan, M.A., Panizza, M., Hamadi, N.B., Ammar, S., 2015. Complete removal of AHPS synthetic dye from water using new electro-fenton oxidation catalyzed by natural pyrite as heterogeneous catalyst. Journal of Hazardous Materials 297, 34-41.

Li, Y., Yao, B., Chen, Y., Zhou, Y., Duan, X., 2023. Metal-organic frameworks (MOFs) as efficient catalysts for electro-Fenton (EF) reactions: Current progress and prospects. Chemical Engineering Journal 463, 142287.

Liu, G., Jiang, W., Wang, Y., Zhong, S., Sun, D., Liu, J., Li, F., 2015. One-pot synthesis of Ag@Fe_3O_4/reduced graphene oxide composite with excellent electromagnetic absorption properties. Ceramics International 41, 4982-4988.

Martone, L., Minella, M., Minero, C., Sordello, F., Vione, D., 2022. Effective degradation of ibuprofen through an electro-Fenton process, in the presence of zero-valent iron (ZVI-EF). Journal of Cleaner Production 367, 132894.

Pan, F., Yang, J., Cai, J., Liu, L., 2021. Heterogeneous Fenton-like oxidative degradation of sulfanilamide catalyzed by RuO_2-rectorite composite. Research On Chemical Intermediates 47, 4595-4611.

Qi, H., Shi, X., Liu, Z., Yan, Z., Sun, Z., 2023. In situ etched graphite felt modified with $CuFe_2O_4$/Cu_2O/Cu catalyst derived from CuFe PBA for the efficient removal of sulfamethoxazole through a heterogeneous electro-Fenton process. Applied Catalysis B: Environmental 331, 122722.

Qiu, B., Hu, Y., Tang, C., Chen, Y., Cheng, J., 2021. Simultaneous mineralization of 2-anilinophenylacetate and denitrification by Ru/Fe modified biocathode double-chamber microbial fuel cell. Science of the Total Environment 792, 148446.

Qiu, B., Hu, Y., Tang, C., Chen, Y., Cheng, J., 2022. Degradation of diclofenac via sequential reduction-oxidation by Ru/Fe modified biocathode dual-chamber bioelectrochemical system: Performance, pathways and degradation mechanisms. Chemosphere 291, 132881

Rao, T., Ma, X., Yang, Q., Cheng, S., Ren, G., Wu, Z., Sirés, I., 2022. Upgrading the peroxi-coagulation treatment of complex water matrices using a magnetically assembled mZVI/DSA anode: Insights into the importance of ClO radical. Chemosphere 303, 134948.

Rokhina, E.V., Lahtinen, M., Nolte, M.C.M., Virkutyte, J., 2009. The influence of ultrasound on the RuI3-catalyzed oxidation of phenol: Catalyst study and experimental design. Applied Catalysis B: Environmental 87, 162-170.

Sathishkumar, P., Meena, R.A.A., Palanisami, T., Ashokkumar, V., Palvannan, T., Gu, F.L., 2020. Occurrence, interactive effects and ecological risk of diclofenac in environmental compartments and biota - a review. Science of the Total Environment 698, 134057.

Shao, D., Li, W., Wang, Z., Yang, C., Xu, H., Yan, W., Yang, L., Wang, G., Yang, J., Feng, L., Wang, S., Li, Y., Jia, X., Song, H., 2022. Variable activity and selectivity for electrochemical oxidation wastewater treatment using a magnetically assembled electrode based on Ti/PbO_2 and carbon nanotubes. Separation and Purification Technology 301, 122008.

Sharafee Shamsudin, M., Taufik Mohd Din, A., Sellaoui, L., Badawi, M., Bonilla-Petriciolet, A., Ismail, S., 2023. Characterization, evaluation, and mechanism analysis of the functionalization of kaolin with a surfactant for the removal of diclofenac from aqueous solution. Chemical Engineering Journal 465, 142833.

Shen, M., Li, W., Chen, F., Chen, L., Chen, Y., Chen, S., Ren, S., Han, D., 2023. A ratiometric electrochemical sensor for bisphenol A detection based on Ag@Fe_3O_4-rGO composite. Microchemical Journal 186, 108315.

Shi, R., Wang, X., Zhou, G., 2023. Electronic metal − support interaction directed electron-deficient nanoparticulate Ru on Ti_3C_2 MXene-derived TiO_2 nanoflowers for robust benzene semi-hydrogenation. Applied Surface Science 624, 157159.

Tan, L., Liu, Y., Zhu, G., Fan, X., Quan, X., 2023. Metal-free electro-Fenton degradation of perfluorooctanoic acid with efficient ordered mesoporous carbon catalyst. Science of the Total Environment 875, 162725.

Wang, Y., Liu, Y., Li, X., Zeng, F., Liu, H., 2013. A highly-ordered porous carbon material based cathode for energy-efficient electro-Fenton process. Separation and Purification Technology 106, 32-37.

Wei, T., Zhang, Y., Wang, H., Li, H., Fang, T., Wang, Z., Dai, Z., 2023. Self-assembled electroactive MOF − magnetic dispersible aptasensor enables ultrasensitive microcystin-LR detection in eutrophic water. Chemical Engineering Journal 466, 142809.

William S. Hummers, J., Richard E. Offeman, 1958. Preparation of Graphitic Oxide. Journal of the American Chemical Society, 1339.

Wojcieszyńska, D., Łagoda, K., Guzik, U., 2023. Diclofenac Biodegradation by Microorganisms and with Immobilised Systems—A Review. Catalysts 13, 412.

Xu, P., Xie, S., Liu, X., Wang, L., Jia, X., Yang, C., 2022. Electrochemical enhanced heterogenous activation of peroxymonosulfate using $CuFe_2O_4$ particle electrodes for the degradation of diclofenac. Chemical Engineering Journal 446, 136941.

Ye, M., Zhang, C., Liu, Z., Li, H., Fu, Z., Zhang, H., Wang, G., Zhang, Y., 2023. E-waste derived CuAu bimetallic catalysts supported on carbon cloth enabling effective degradation of bisphenol A via an electro-Fenton process. Separation and Purification Technology 305, 122507.

Zhang, C., Li, F., Zhang, H., Wen, R., Yi, X., Yang, Y., He, J., Ying, G., Huang, M., 2021. Crucial roles of 3D–MoO$_2$–PBC cocatalytic electrodes in the enhanced degradation of imidacloprid in heterogeneous electro–Fenton system: Degradation mechanisms and toxicity attenuation. Journal of Hazardous Materials 420, 126556.

Zhang, J., Qiu, S., Feng, H., Hu, T., Wu, Y., Luo, T., Tang, W., Wang, D., 2022. Efficient degradation of tetracycline using core–shell Fe@Fe$_2$O$_3$-CeO$_2$ composite as novel heterogeneous electro-Fenton catalyst. Chemical Engineering Journal 428, 131403.

Zhang, Q., Yu, L., Xu, C., Zhao, J., Pan, H., Chen, M., Xu, Q., Diao, G., 2019. Preparation of highly efficient and magnetically recyclable Fe$_3$O$_4$@C@Ru nanocomposite for the photocatalytic degradation of methylene blue in visible light. Applied Surface Science 483, 241-251.

Zhang, Y., Jiao, Z., Hu, Y., Lv, S., Fan, H., Zeng, Y., Hu, J., Wang, M., 2017. Removal of tetracycline and oxytetracycline from water by magnetic Fe$_3$O$_4$@graphene. Environmental Science and Pollution Research 24, 2987-2995.

Zhang, Y., Liu, M., Pan, S., Yu, L., Zhang, S., Liu, R., 2022. A magnetically induced self-assembled and label-free electrochemical aptasensor based on magnetic Fe$_3$O$_4$/Fe$_2$O$_3$@Au nanoparticles for VEGF165 protein detection. Applied Surface Science 580, 152362.

Zhang, Y., Zhang, C., Shao, D., Xu, H., Rao, Y., Tan, G., Yan, W., 2022. Magnetically assembled electrodes based on Pt, RuO$_2$-IrO$_2$-TiO$_2$ and Sb-SnO$_2$ for electrochemical oxidation of wastewater featured by fluctuant Cl- concentration. Journal of Hazardous Materials 421, 126803.

Zhou, H., Dong, H., Wang, J., Chen, Y., 2020a. Cobalt anchored on porous N, P, S-doping core-shell with Generating_activating dual reaction sites in heterogeneous electro-fenton process. Chemical Engineering Journal 406,125990,

Zhou, X., Xu, D., Chen, Y., Hu, Y., 2020b. Enhanced degradation of triclosan in heterogeneous E-Fenton process with MOF-derived hierarchical Mn/Fe@PC modified cathode. Chemical Engineering Journal 384, 123324.

Zou, Y., Qi, H., Sun, Z., 2022. In-situ catalytic degradation of sulfamethoxazole with efficient CuCo−O@CNTs/NF cathode in a neutral electro-Fenton-like system. Chemosphere 296, 134072.